Acta Cybernetica **20** (2011) 189–206.

Parameter Estimation of Flow-Measurement in Digital Angiography*

Krisztian Veress† and Tibor Csendes†

Abstract

The purpose of angiographic procedures used in cardiovascular interventions is to classify the patient's potential of regeneration after strokes caused by dead blood cells in the main arteria. The flow of blood into heart's capillaries is measured using x-ray radiometry with contrastive fluids. One quick and reliable method for estimating this potential could save lives and would allow further treatments to be more accurately planned.

Our task was to fit a 5-parameter Gamma function to the intensity samples extracted from the x-ray angiograms. The estimation of this function's parameters is hard given that the raw data set is heavily polluted with several different types of noise.

Our complete solution has four main parts which have also been successfully verified and validated. First, we propose a solution for eliminating the noise by applying a specially designed moving window Gauss filter. Secondly, we have designed an algorithm for computing a good initial guess for the Levenberg-Marquardt optimizer in order to achieve the required precision. Third, an algorithm is proposed for selecting significant points on the smoothed data set with an interval-based classification method. Finally, we apply the LM algorithm to compute the solutions in a nonlinear least squares way.

We have also formulated an algorithm based on interval arithmetic which can be effectively used for comparing nonlinear least-squares fit results and assign goodness values based on their residuals. This method has been used for measuring improvements during the development.

We must emphasize that the proposed algorithms are distinct, they can be used in other applications together or separately since they are generally applicable, they do not depend on specialties of the presented application.

Keywords: numerical analysis, optimization, parameter estimation, gamma function

*This work was supported by the national grant TAMOP-4.2.1/B-09/1/KONV-2010-0005
†Institute of Informatics, University of Szeged E-mail: {verkri,csendes}@inf.u-szeged.hu

DOI: 10.14232/actacyb.20.1.2011.13

1 Introduction

The digital substraction angiography [17] used in medical surgery is one kind of an image recording and processing method where panoramic x-ray images are taken while contrastive x-ray fluid [8] is injected into the patient's heart's main arteria. The x-ray fluid flow is similar to blood-flow [11], thus the amount of blood that can reach the critical region can be measured. The goal is to estimate the patient's survival chances who has recently survived a stroke, being dead blood cells removed by means of a surgery intervention. There is a high correlation between these and the regeneration ratio (perfusion parameter) of his/her cardiac muscle [1], [22].

X-ray panoramic images are recorded at a rate of 15 fps for 10 to 15 seconds yielding 150 to 225 frames as digital substraction angiograms [17]. The surgerer in charge selects the critical cardiac muscle region as the Region of Interest (ROI) [21] on the first couple of frames. The intensity of the x-ray fluid can be computed on each frame [3] by calculating the average intensity of the interior pixels in that ROI. In this way, an aggregate intensity value for each frame brings on a time-series ($M(t)$) which is going to be our input. Two examples are shown in Figure 1.

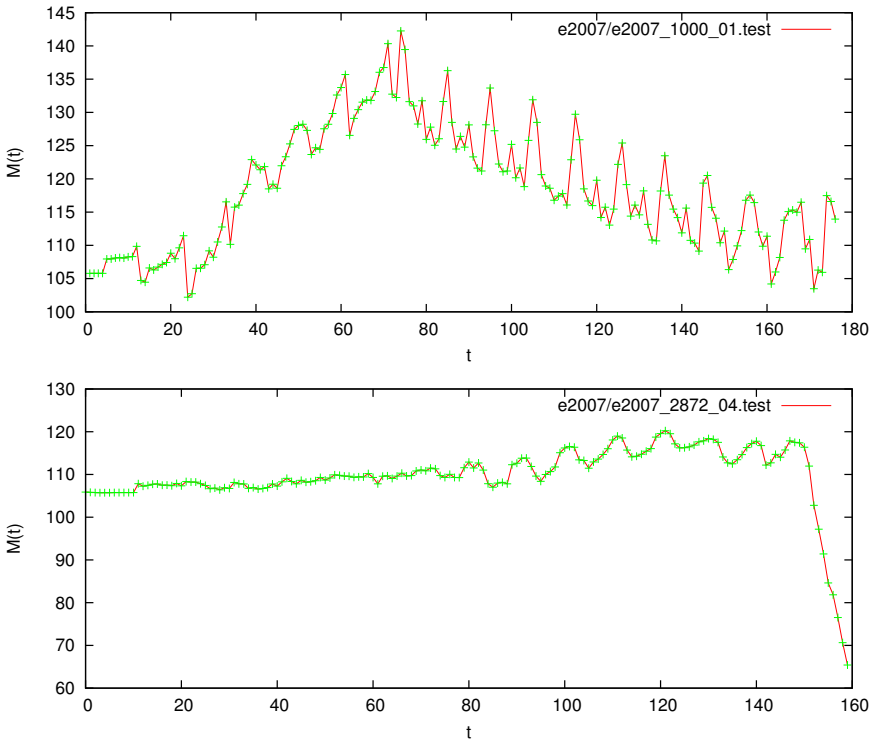

Figure 1: One valid and one erronous input time-series of x-ray intensities

1.1 Modelling flow dynamics

Our main task was to characterize the x-ray fluid flow in blood vessels by means of numerical values. Several theoretical formulations have been proposed to explain the shape of peripheral indicator dilution curves [24], [25]. One expression proposed by Evans [5] and examined by Howard [13] has a graphical representation which bears a remarkable resemblance to indicator dilution curves without recirculation. This function can be expressed in the original form

$$H(t) = K_s(t - AT)^{\alpha} e^{-\frac{t - AT}{\beta}} + Z_l, \tag{1}$$

being $K_s > 0$ a constant scale factor, $AT > 0$ the appearance time, $Z_l > 0$ an offset, and $\alpha, \beta > 0$ the rising and descending slope shape parameters. To have a quick overview of this mathematical model, we have plots with different parameter sets in Figure 2.

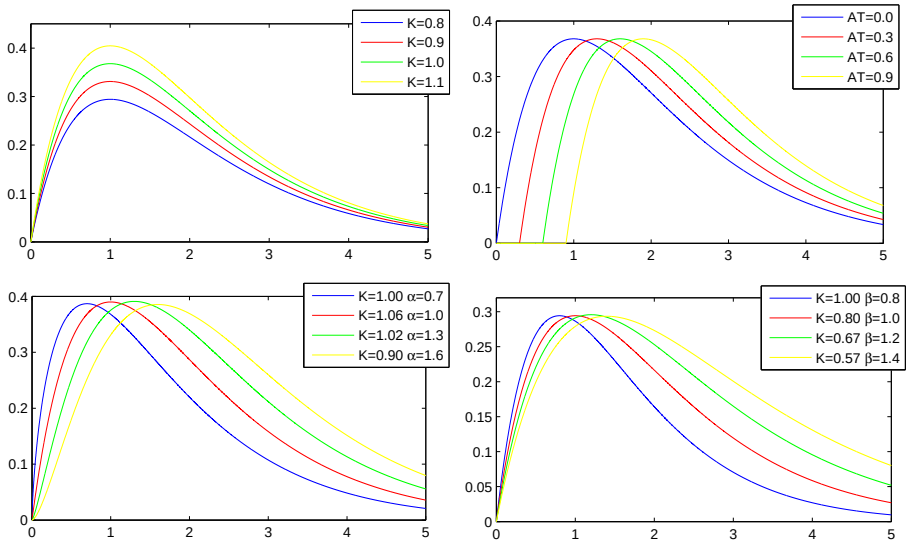

Figure 2: The effect of changing single parameters of $H(t)$

The AT parameter specifies the time when the contrastive fluid has been injected while Z_l and K_s are the base intensity and intensity scaling values of the x-ray device. The slope parameters describe the way blood can enter and exit the cardiac muscle. Since well-studied physiological meanings are to be abstracted from these numerical parameters [13], estimating them precisely and accurately is a must.

The main objective was to efficiently fit $H(t)$ to the initial samples $M(t)$ with high confidence regarding the nature of the consequences our results could introduce. Early studies showed that our inputs can be more precisely modeled with a

slightly modified version of $H(t)$:

$$G(t) = \left\{ \begin{array}{ll} Z_l & \mid \ AT < t \\ & \\ H(t) = K_s(t-AT)^{\alpha} e^{\frac{-(t-AT)}{\beta}} + Z_l & \mid \ AT \geq t \end{array} \right\}, \tag{2}$$

What we have now, is a formulation of a non-linear parameter estimation problem where the measured data is $M(t)$ and the model is $G(t)$. There are several methods for solving such problems [6],[14],[23] among which we have selected the Least Squares Estimation procedure. To be more precise, we are going to use the Levenberg-Marquardt algorithm [15], [19], minimizing the difference between the model and sample values in a nonlinear least squares way [7], [16]:

$$Z_{res} = \sum_{i=1}^{n} \left(G(t_i) - M(t_i)\right)^2 \rightarrow \min . \tag{3}$$

1.2 Normalizing residual squares

After estimating the regression parameters, an essential aspect of the analysis is to test the appropriateness of the overall model. To declare a fit 'good' or 'bad', the sole sum of the residuals (Z_{res}) are not reasonably satisfactory, since a 'better' fit can have higher Z_{res} values than a 'worse' one caused by heavy noise or badly scaled sample.

Widely used techniques such as proportion of variance, chi-square and covariance matrix calculations showed nothing better. Since Z_{res} can be arbitrarily large, we propose a method for scaling these values into any chosen interval.

Let $\mathbf{f}, \mathbf{m} \in \mathbb{R}^n$, $\mathbf{f}$ be the *vector* of our fitted values, $\mathbf{m}$ the measurement *vector*, $g_l, m_l \in \mathbb{R}$ lower, and $g_u, m_u \in \mathbb{R}$ upper bound values. Then $\forall i \in 1, \ldots, n$

$$\begin{array}{rrr} \mathbf{m}_i \in [m_l, m_u], & m_l \leq m_u, & m_l, m_u \in [0, 255], \\ \mathbf{g}_i \in [g_l, g_u], & g_l \leq g_u, & g_l, g_u \in [0, 255], \end{array}$$

which results the following inclusion (based on interval arithmetic):

$$(\mathbf{g}_i - \mathbf{m}_i) \in [g_l, g_u] - [m_l, m_u] \in [g_l - m_u, g_u - m_l].$$

From interval arithmetic we know that for any $f : \mathbb{R}^n \mapsto \mathbb{R}$ function, its *natural interval extension* is given by the interval-valued function in the form

$$F : [\mathbb{R}^n] \mapsto [\mathbb{R}] \ \text{ where } \ F([x]) \supseteq \{f(y) \mid y \in [x]\}$$

and can be formulated by replacing each value with its thickest encasing interval:

$$x \in \mathbb{R} \ \mapsto \ [x, x] \in [\mathbb{R}].$$

Now we can easily compute the natural interval extension of Z_{res}:

$$\begin{aligned} Z_{res} &= \sum_{i=1}^{n} \left(G(t_i) - M(t_i)\right)^2 = \sum_{i=1}^{n} \left(\mathbf{g}_i - \mathbf{m}_i\right)^2 \\ &\in \sum_{i=1}^{n} \left([g_l - m_u, g_u - m_l]\right)^2 \in \sum_{i=1}^{n} \left([0, \max\left((g_l - m_u)^2, (g_u - m_l)^2\right)]\right) \\ &\in [0, n \max\left((g_l - m_u)^2, (g_u - m_l)^2\right)]. \end{aligned}$$

which implies that

$$\widehat{Z}_{res} = \frac{1}{n} \frac{Z_{res}}{\max\left((g_l - m_u)^2, (g_u - m_l)^2\right)} \in [0, 1]. \tag{4}$$

The plotted original Z_{res} and normalized $\widehat{Z}_{res}$ values for different inputs are shown in Figure 3 (smaller value means better accuracy). Note that the normalized values are more scattered than the original ones meaning that normalization pushes away 'bad' and 'good' fits.

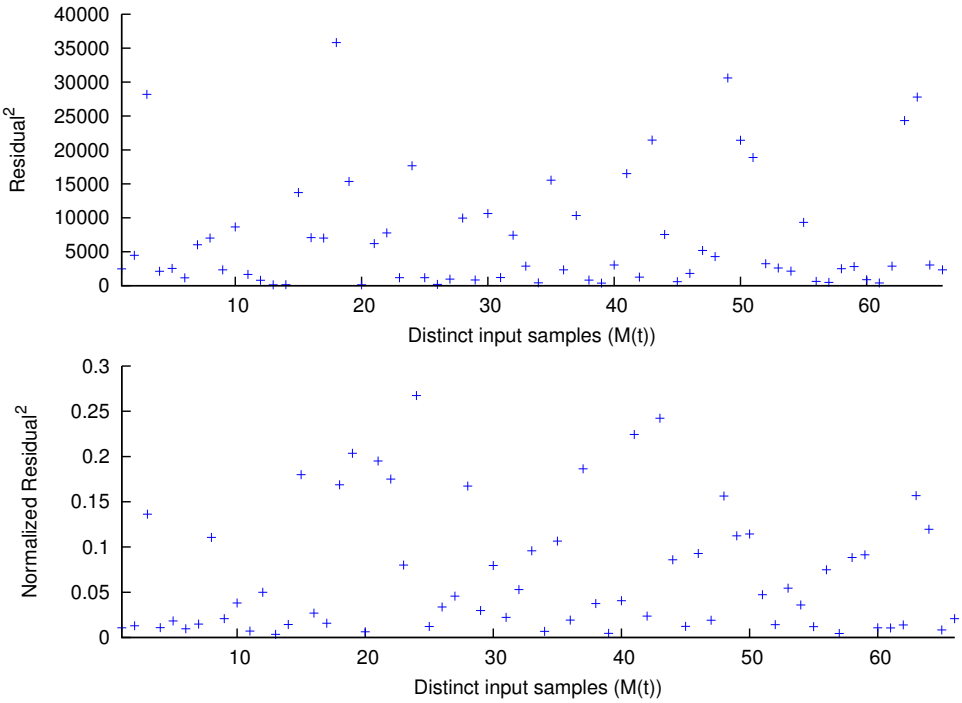

Figure 3: Original and normalized residuals on 66 different $M(t)$ samples

1.3 Results on the initial samples

To evaluate our solution we had 66 real life, anonymous medical samples at our disposal. We must emphasize that these samples contain noises from uncountable sources [10] (i.e. unprecise recording, unprecise fluid injection [8], x-ray device's auto-intensity regulation [9], image processing bugs [18]) and our effort in figuring out suitable noise models was a fool's errand.

We have implemented our solution in C++ by making the most of the Insight Toolkit [26]. On the first attempt we tried to directly fit the model (2) to our input using the mentioned LMA algorithm. Since the latter is an iterative curve-fitting method, we had to feed it with a suitable initial guess vector which was chosen for the following:

$$P_0 = (K_s, AT, \alpha, \beta, Z_l) = (0.02, 34.0, 3.3, 11, 1, 106.0)$$

Based on our statistic analyses P_0 describes a nearly-optimal estimator for a well-conducted, unnoisy, and error-free measurement sample. Since the results were really bad (concerning either performance or precision), we classified each fit in a graphical way into *appropriate* and *inappropriate fit* classes (see Figure 4), separately computed the normalized residuals and lastly matched these two properties.

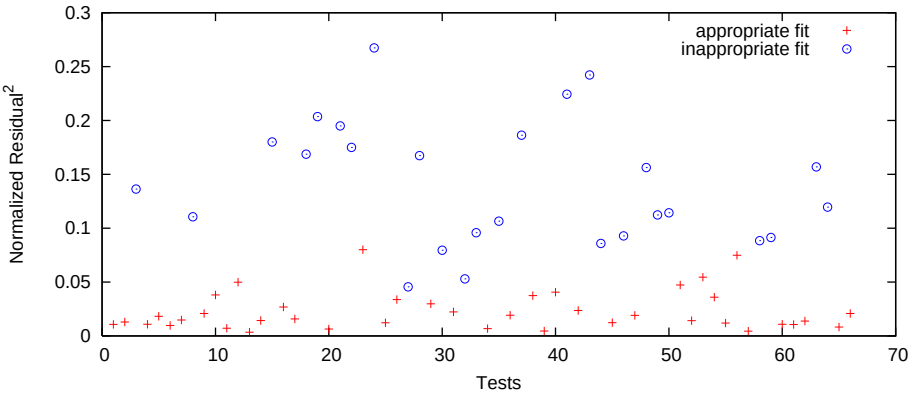

Figure 4: Normalized results on the test database (naive fit)

In Figure 4 a somewhat sharp interface showed up between appropriate and inappropriate classes from which we may conclude that there exist a high correlation between our normalized values and the optimality of the estimators.

However, we must recognize that not every inappropriatedly classified sample is a clearly wrong measurement which means that the LMA algorithm should be fined-tuned and other pre-, and post-processing phases should be included in our complete solution.

2 Noise filtering

In order to achieve better results, we have decided to apply a noise filtering algorithm whose primary goal was to eliminate spikes and produce a smoothed sample. Simple filters like median and arithmetic mean moving-window filters did not perform well on all types of measurements.

The chosen filtering algorithm is a general Gaussian moving window average type [12] filter with specially designed weights and variable length window size. The weights are designed to be precomputable given an initial sample, and not to introduce undesired offsets and scaling on the input values:

$$M^*(t_i) = \sum_{j=i-L_w}^{i+L_w} \frac{M(t_j)}{2L_w+1}\, w_j \quad \text{if} \quad L_w \leq t_i \leq |M(t)| - L_w,$$

where $\forall j \in [i-L_w, i+L_w]$, and the weights are:

$$w_j = e^{-(t_j-t_i)^2/(2L_w+1)} \frac{2L_w+1}{\sum_{j=i-L_w}^{i+L_w} e^{-(t_j-t_i)^2/(2L_w+1)}}.$$

By selecting the weights in this way, it is guaranteed that $\forall i \in [1, n]$:

$$\sum_{j=i-L_w}^{i+L_w} w_j = \sum_{j=i-L_w}^{i+L_w} \left(e^{-(t_j-t_i)^2/(2L_w+1)} \frac{2L_w+1}{\sum_{j=i-L_w}^{i+L_w} e^{-(t_j-t_i)^2/(2L_w+1)}} \right) = 2L_w + 1.$$

Generally speaking our proposed weighting method gives us a (not arithmetic) mean moving window filter with Gaussian weights. The optimal window size has been selected by generating a histogram for all possibly usable window sizes for all inputs in our database resulting the value 33.

This modification of the original smoothing filter has the same advantages as to the Savitzky-Golay [20] filter because it also tends to preserve features of the distribution such as relative maxima, minima and width, which are usually 'flattened' by other adjacent averaging techniques. However, further researches should be conducted to compare the performance, stability and applicability of these two filters and select the most appropriate one.

Our proposed filtering algorithm can successfully be used on any one-dimensional sample since weights depend only on the measurement vector and the optimal window size can also be found in the above way.

2.1 Smoothing results

In Figure 5 we present four different initial samples and the result of our proposed smoothing filter. One can see that our filter is not sensitive to radidly changing curves or spikes and keeps the dominant part of the input signal.

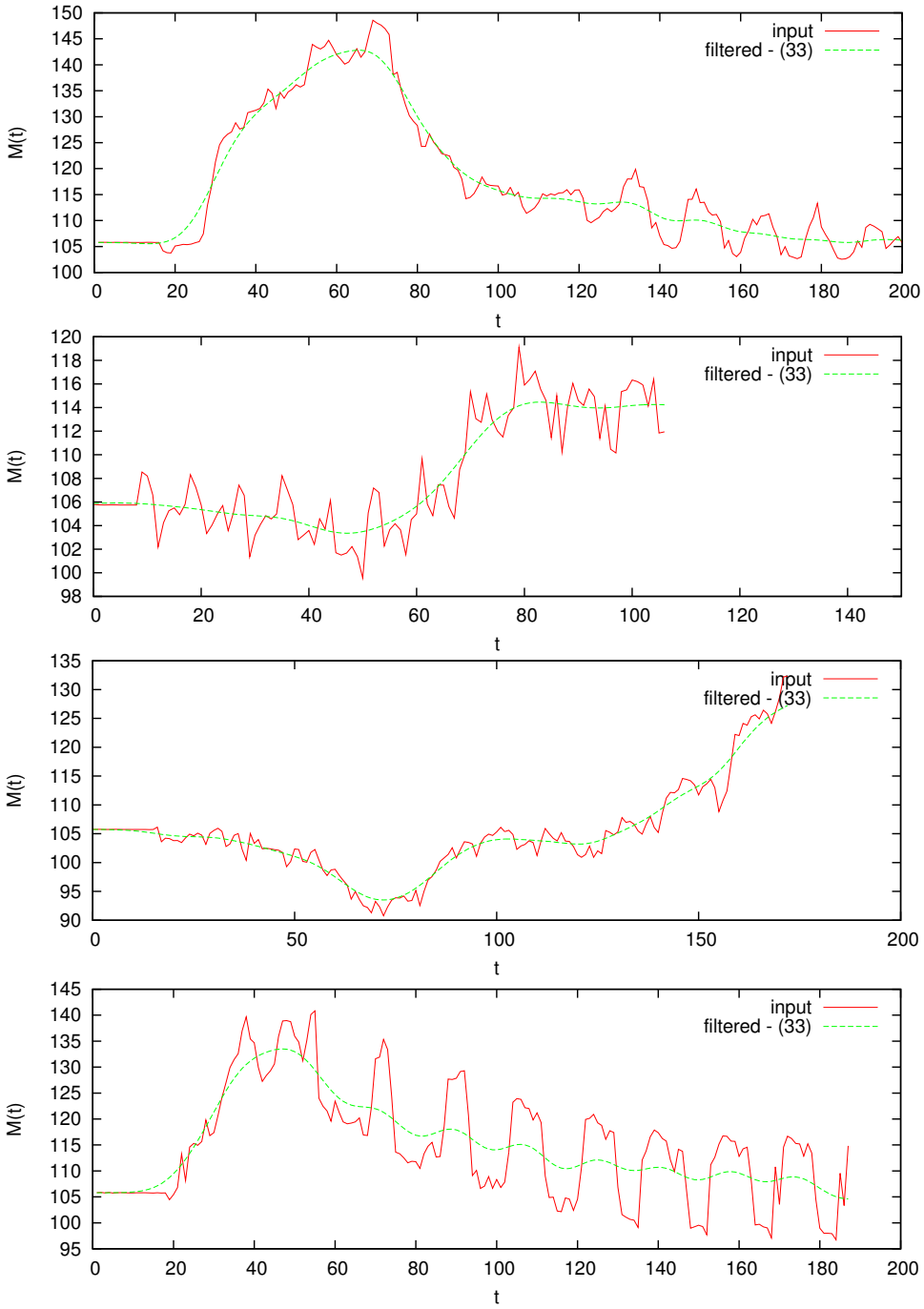

Figure 5: Smoothing filter results on real medical samples

2.2 Results on the filtered samples ($M^*(t)$)

We modified the NLLS LMA minimizer's objective function as to minimize the difference between the model ($G(t)$ and the **filtered sample** ($M^*(t)$). Table 1 shows aggregate statistics about the results generated on the 66-element test database.

Table 1: Numerical results of the LMA algorithm on $M(t)$ and $M^*(t)$ samples

$M(t)$	min	max	mean	median
iterations:	3	9999	3796.09	46
Z_{res}:	121.84	35815.86	7010.51	2811.72
$\widehat{Z}_{res}$:	0.0034	0.267	0.069	0.037
CPU time (s):	0.01	7.22	2.03	0.21

$M^*(t)$	min	max	mean	median
iterations:	4	9998	2158.71	45
Z_{res}:	122.09	30084.45	3730.36	2480.72
$\widehat{Z}_{res}$:	0.0034	0.255	0.048	0.034
CPU time (s):	0.01	7.34	1.13	0.07

One can see that when using $M^*(t)$ as reference, half the time is required to achieve double precision (compare Z_{res} values). The normalized values ($\widehat{Z}_{res}$) have also significantly decreased which means better fits. As before, we evaluated all curve-fitting results, classified them, and plotted the $\widehat{Z}_{res}$ values (Figure 6).

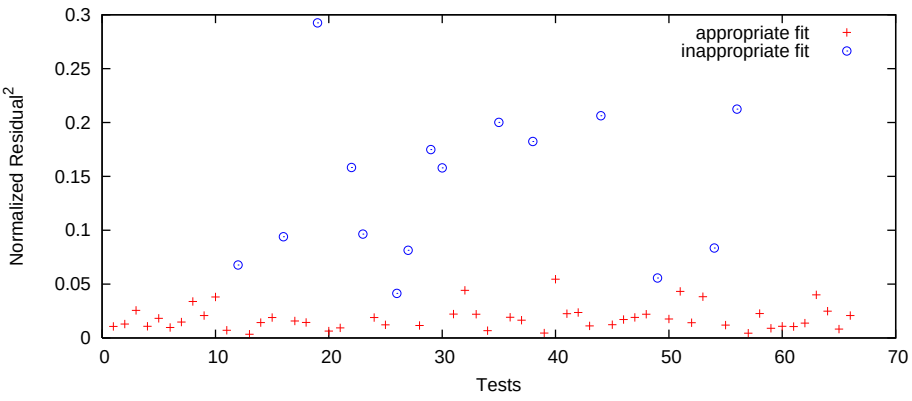

Figure 6: Normalized results on the test database (filtered fit)

Notice that the bad fit count decreased and the interface between appropriate and inappropriate classes sharpened which let us conclude that using the filtered signal is far better than using the original one.

3 Initial guess computation for LMA

Until now, we used a static, constant initial vector P_0 for the LM algorithm. Given the nature of the source experiments, real solution vectors are expected to be scattered in space. Scattering means greater search space, which indicates that a static initial vector for the LMA is in general a bad choice.

We propose an algorithm which is able to dynamically compute an excellent approximation of the estimator based on the filtered sample in $\mathcal{O}(1)$ time and $\mathcal{O}(n)$ space. Further advantage of our proposed algorithm is that is can also be used in other applications where the same (or analytically equivalent) model is applied.

It is known, that fluid injection is scheduled to be one second after the start of the recording, so the estimation of the Z_l parameter is trivial; we have to compute the arithmetical mean of the first 15 values of $M^*(t)$.

To estimate the other 4 parameters, we have computed the first order $H'(t)$ and second order $H''(t)$ derivatives of $H(t)$ and solved the $H'(t) = 0$ and $H''(t) = 0$ equations for identifying minimizer, maximizer and inflection points. The results showed that $H(t)$ has only one single maximum point (at t_{max}), and two inflection points (at $t_{i,1}$ and $t_{i,2}$) which can be expressed with α,β, and AT:

$$\begin{aligned} t_{max} &= \alpha\beta + AT, \\ t_{i,1} &= \alpha\beta - \sqrt{\alpha}\beta + AT, \\ t_{i,2} &= \alpha\beta + \sqrt{\alpha}\beta + AT. \end{aligned}$$

In this way, if we were able to produce a good estimation for t_{max}, $t_{i,1}$ and $t_{i,2}$, by solving the above nonlinear systems of equations we would acquire good estimations for AT, α, and β. However, the solution of this NLP problem is hard, complex NLP solvers are likely to introduce further errors, that is why we have chosen a simpler and faster heuristic method.

Taking the above three equations the following expressions can be derived:

$$\alpha = \frac{(t_{max} - AT)^2}{(t_{max} - t_{i,1})^2} = \frac{(t_{max} - AT)^2}{(t_{i,2} - t_{max})^2}, \tag{5}$$

$$\beta = \frac{(t_{max} - t_{i,1})^2}{t_{max} - AT} = \frac{(t_{i,2} - t_{max})^2}{t_{max} - AT}. \tag{6}$$

Since the AT parameter (the x-ray fluid appearance time) can easily be detected on $M^*(t)$, and given the t_{max} and one of the $t_{i,1}$ and $t_{i,2}$ values, α and β are directly computable using equations (5) and (6). The estimation of the AT parameter is done by combining zero and first order assumptions on the ideal model:

$$\begin{aligned} AT &\approx \frac{1}{3}\arg\max_t \left(M^{*'}(t) = 0\right) + \frac{1}{3}\arg\max_t \left(M^*(t) = Z\right) + \\ &+ \frac{1}{3}\arg\min_t \left(M^*(t) > Z\right). \end{aligned} \tag{7}$$

Last but not least, an estimation for the K_s parameter must be given. This scaling is determined by the maxima of $G(t)$ (2). Given that

$$H(t_{max}) = (\alpha\beta)^{\alpha} e^{-\frac{\alpha\beta}{\beta}} + Z = (\alpha\beta)^{\alpha} e^{-\alpha} + Z,$$

an approximation for K_s can be formulated as

$$K_s \approx \frac{\max(M^*(t)) - Z}{(\alpha\beta)^{\alpha} e^{-\alpha}}. \tag{8}$$

Summarizing our method, we must

1. localize the maximum point t_{max} and maxima of $M^*(t)$,
2. localize at least one inflection point ($t_{i,1}$ and/or $t_{i,2}$) by searching discrete approximated roots of $M^{*'}(t)$,
3. compute an approximation for AT given the equation 7,
4. compute approximations for α, β, and K_s using equations 5, 6, and 8.

One may wonder how good estimation is computed by the proposed algorithm. To astonish the reader, we present some numerical and graphical results. Table 2 shows the general and normalized residuals as if the initial guess was our final solution vector.

Table 2: Computed initial guess vector evaluation

	min	max	mean	median
Z_{res}:	235.88	17085.28	4009.98	343.64
$\widehat{Z}_{res}$:	0.0090	0.2379	0.0436	0.02719
CPU time (s):	0.01	0.26	0 .025	0.02

If compared to Table 1, it is in full view that the newly proposed algorithm performs much better than using the LMA with static starting point. Of course, being an initial vector we can achieve further improvements (Table 3).

Table 3: LMA results using computed initial guess

$M^*(t)$	min	max	mean	median
Z_{res}:	120.45	11245.8	3210.77	134.66
$\widehat{Z}_{res}$:	0.007	0.231	0.0316	0.0187
CPU time (s):	0.01	2.54	0.42	0.05

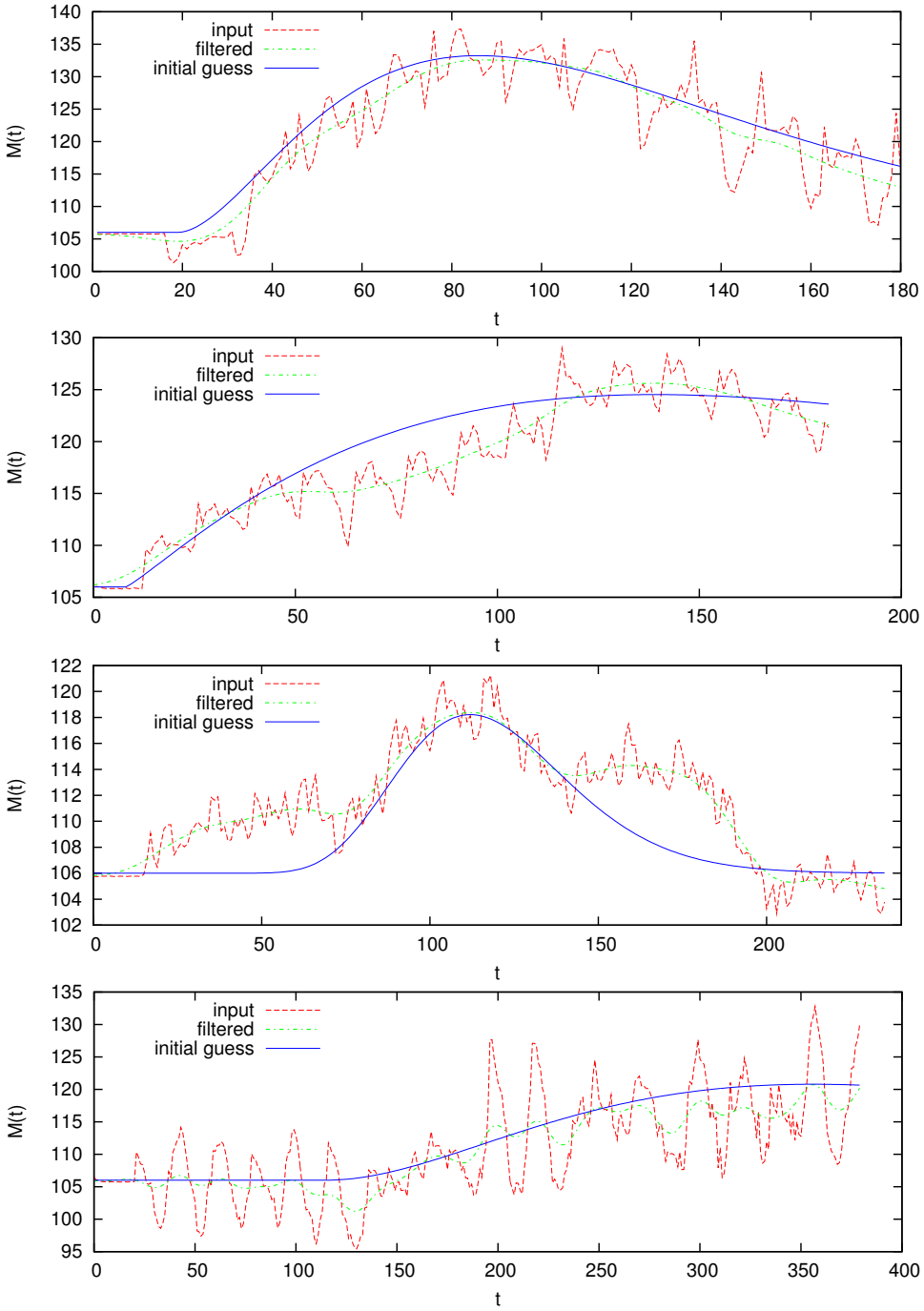

Figure 7: Initial guess computation results on the test database

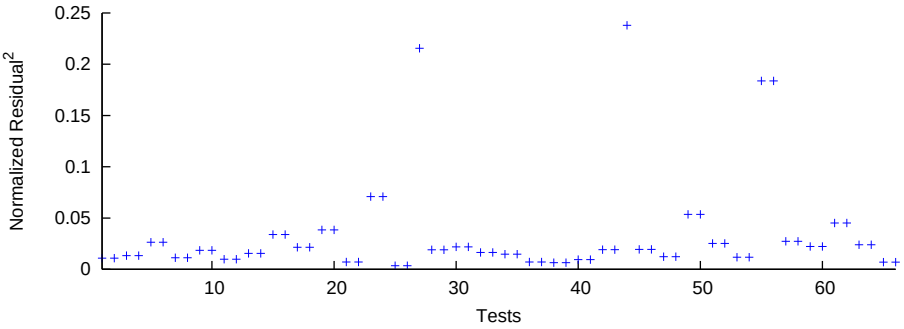

Figure 8: Normalized results with dynamic initial vector

In Figure 7 four results are shown along with the original and filtered samples. Notice that how diverse could be the shape of the input measurements. In Figure 8 showing the normalized residuals for the new approach, each fit has been classified as appropriate, higher values indicate wrong samples which must be dropped or re-recorded. At this point, the required efficiency and precision has been achieved.

4 Significant point selection

Although we could have stopped at this point, we was wondering how could we improve the physiological accuracy (not the numerical) of our solution. In order to achieve this new goal, the compression [2] of the input signal was the first step. All 200 (on average) intensity values in the filtered sample are too much for our model's 5 parameters [4]. Using less measurement values (about 20), we expected that our curve-fitting would be even more faster and accurate in a biological sense. The results showed a positive feedback.

Our basic idea was to classify the filtered sample's values as *significant* and *non-informational* points. To select the *significant* ones, we must detect those points where there are sudden changes in $M^*(t)$. Generally speaking, we want to approximates the curve with a polyline. Our point selection scheme is based on the first order discrete derivative of $M^*(t)$:

$$\partial M^*(t) = D_S(t) = \begin{cases} 0 & \text{if } \ t = 1 \\ M^*(t) - M^*(t-1) & \text{otherwise} \end{cases}$$

by dividing its codomain into a pre-defined number of intervals (C_I). The limits for an interval I_i can be computed using the following equations:

$$\begin{aligned} \underline{I_i} &= \min(D_S) + (i-1)\left(\frac{\max(D_S) - \min(D_S)}{C_I}\right), \\ \overline{I_i} &= \min(D_S) + i\left(\frac{\max(D_S) - \min(D_S)}{C_I}\right). \end{aligned}$$

The second part of the point selection is while scanning $D_S(t)$, we track some history on the previously seen values and note those moments where the previous point was located in another interval than the current one. This yields selected points near interval borders.

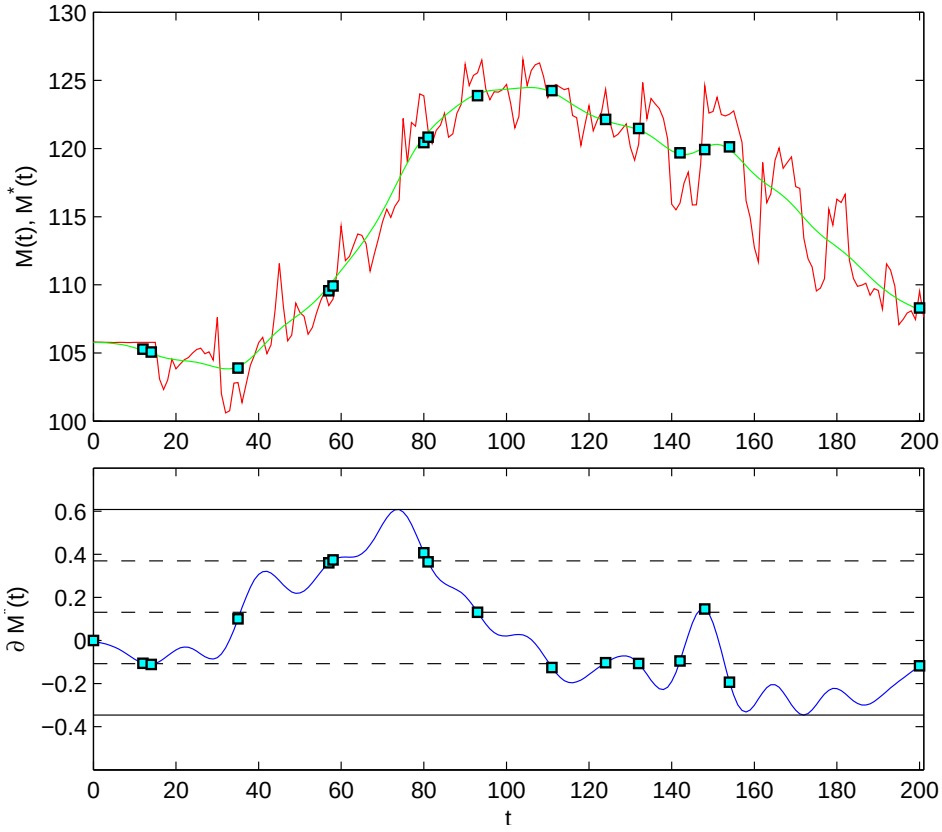

Figure 9: Significant point selection algorithm

The scheme of this method is shown in Figure 9, where the bottom graph shows the codomain of $D_S(t)$ divided into $C_I = 4$ equidistant intervals. The blue squares are the selected *significant* points which are then projected onto the top graph.

Of course, increasing C_I would increase the selected points, since the interval lengths would be smaller yielding more interval-border crossings. The proposed algorithm is designed to be driven by only one parameter – the *target significant point count*. The implementation is designed to select as many points as requested; more requested points mean more accurate approximation but less compression and vice versa. Also take note that our third proposed algorithm can also be used on any kind of a discrete sample in any dimensions.

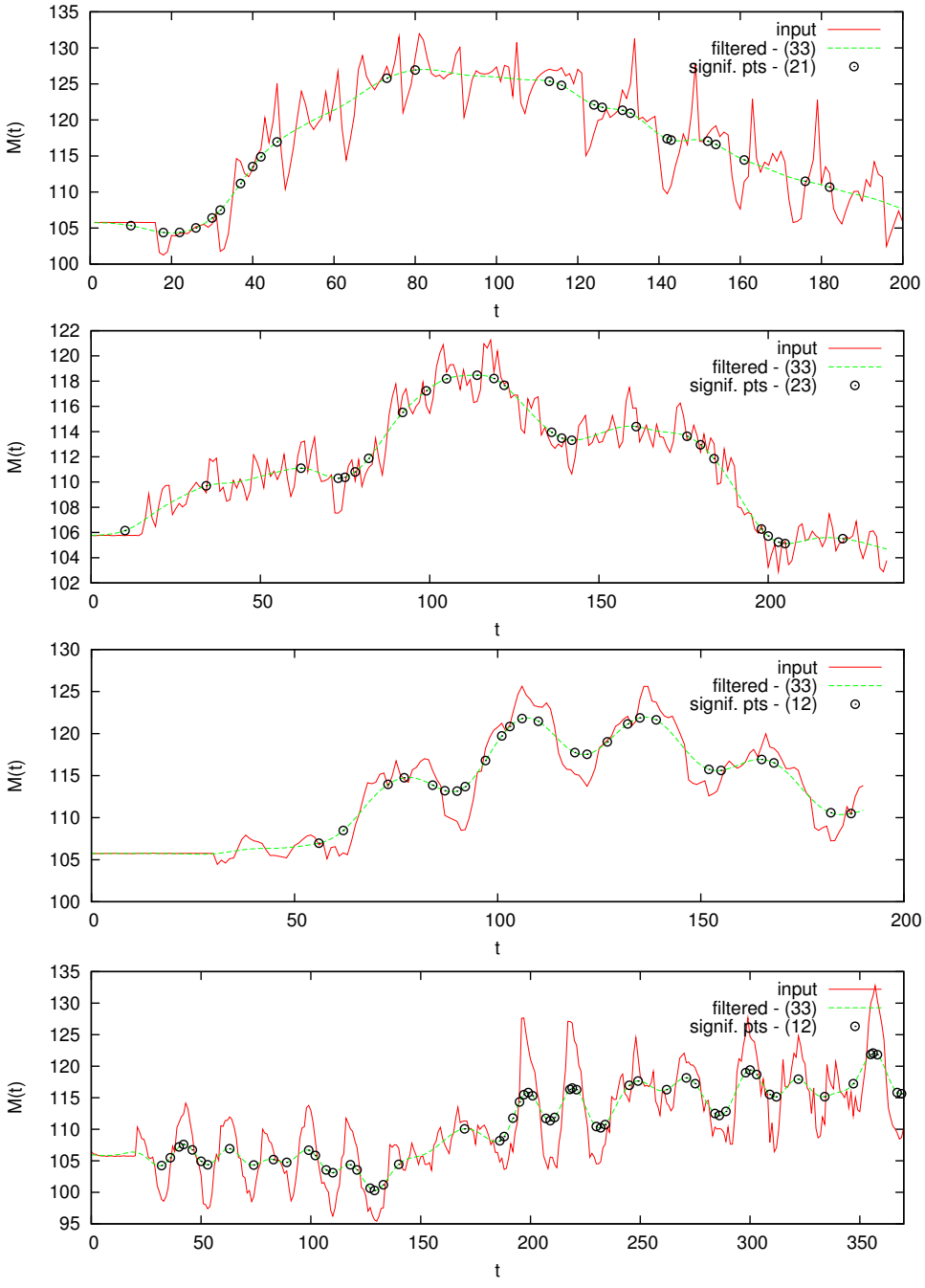

Figure 10: Significant point selection results

5 Final results

To summarize the work, our complex solution consists of a special filter, a pure mathematical initial guess computation algorithm, a measurement compression method and last but not least a NLLS Levenberg-Marquardt solver. This is also the order of their application, so after getting the initial sample, we apply our filter, compute an appropriate initial vector and select significant points using the filtered sample, and apply the LM optimizer with the pre-computed vector on the significant data points as empirical data.

We have successfully applied our solution for all the 66 real measurements at our disposal, selected 4 measurements to be re-recorded, and computed an excellent approximation of the model's parameters for the remaining 62 data sets. These have been validated by surgeons specialized in cardiovascular experiments and interventions at the Cardiovascular Research Laboratory at University of Szeged, Hungary.

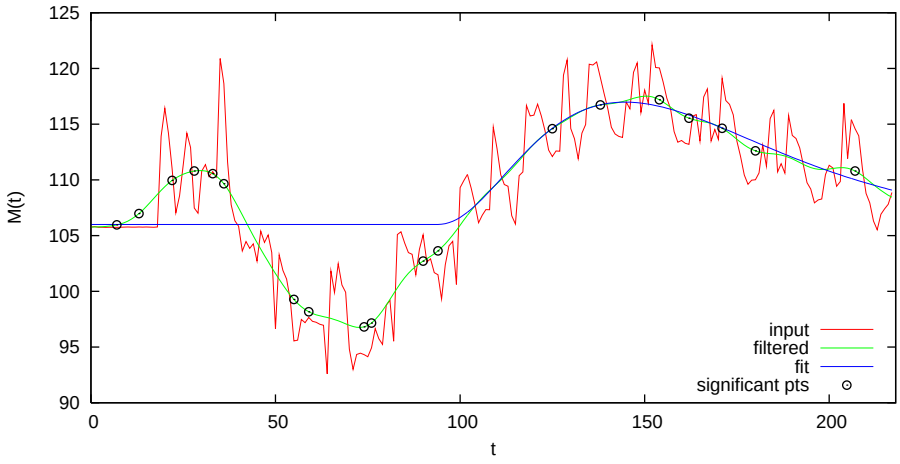

Figure 11: Composite result of a particular fit

Our composite solution technique is able to determine the validity of the measurement, then if it proves to be valid, we provide guaranteed results on any kind of input sample with high precision using no more than 2 seconds of computation time![1]!

Comparing our solution with the time requirements of arranging the patient into the examination room, recording the x-ray video, image processing and ROI selection, we can surely say that our solution is really efficient and also effective enough to incorporate it into real-world devices.

[1] Using an Intel Core 2 T2300, 4 GB RAM based PC

References

[1] Abidov, Aiden, Germano, Guido, and Berman, Daniel. Transient ischemic dilation ratio: A universal high-risk diagnostic marker in myocardial perfusion imaging. *Journal of Nuclear Cardiology*, 14:497–500, 2007.

[2] Ahmedaa, Sabah Mohamed and Abo-Zahhad, Mohammed. A new hybrid algorithm for ecg signal compression based on the wavelet transformation of the linearly predicted error. *Medical Engineering and Physics*, 23:117–126, 2001.

[3] Brown, Lisa Gottesfeld. A survey of image registration techniques. *ACM Computing Surveys*, 24:325–376, 1992.

[4] de Graaf, P., v. Goudoever, J., and Wesseling, K. Compressed storage of arterial pressure waveforms by selection of significant points. *Medical and Biological Engineering and Computing*, 35:510–515, 1997.

[5] Evans, R. L. Two comments on the estimation of blood flow and central volume from dyedilution curves. *J. Appl. Physiol.*, 14(3):457, 1959.

[6] Gao, Zhenxiao, Xiao, Tianyuan, and Fan, Wenhui. Hybrid differential evolution and neldermead algorithm with re-optimization. *Soft Computing*, pages 1–14, 2010.

[7] Ghogho, Mounir, Swami, Ananthram, and Asoke, K.N. Non-linear least squares estimation for harmonics in multiplicative and additive noise. In *Signal Processing*, pages 43–60, 1999.

[8] Gibson, CM., Anshelevich, M., and Murphy, S. Impact of injections during diagnostic coronary angiography on coronary patency in the setting of acute myocardial infarction from the timi trials. *Am J Cardiol.*, 86(12):1378–1379, 2000.

[9] Gibson, CM, Kirtane, AJ, and Murphy, S. Impact of contrast agent type (ionic versus non-ionic) used for coronary angiography on angiographic, electrocardiographic and clinical outcomes following thrombolytic administration in acute mi. *Catheter Cardiovasc Interv.*, 53:6–11, 2001.

[10] Gibson, CM. and Schmig, A. Coronary and myocardial angiography: angiographic assessment of both epicardial and myocardial perfusion. *Circulation*, 109(25):3096–3105, 2004.

[11] Gobbel, Glenn T., Christopher, Dvm, Cann, E., and Fike John, R. 768 measurement of regional cerebral blood flow using ultrafast computed tomography theoretical aspects.

[12] Haddad, R.A and Akansu, A.N. A class of fast gaussian binomial filters for speech and image processing. *IEEE Transactions on Acoustics, Speech and Signal Processing*, 39:723–727, 1991.

[13] Howard K. Thompson, Jr., Frank Starmer, C., Whalen, Robert E., and McIntosh, Henry D. Indicator transit time considered as a gamma variate. *Circulation Research, American Heart Association*, 15:502–515, 1964.

[14] Lee, Sik-Yum and Zhu, Hong-Tu. Maximum likelihood estimation of nonlinear structural equation models. *Psychometrika*, 67:189–210, 2002.

[15] Lourakis, Manolis I. A. and Argyros, Antonis A. Is levenberg-marquardt the most efficient optimization algorithm for implementing bundle adjustment?, 2005.

[16] Madsen, Kaj, Bruun, Hans, and Imm, Ole Tingleff. Methods for non-linear least squares problems. Technical report, 2004.

[17] Meijering, E.H.W., Niessen, W.J., and Viergever, M.A. Retrospective motion correction in digital subtraction angiography: A review. *IEEE Transactions on Medical Imaging*, 18:2–21, 1999.

[18] Meijering, E.H.W., Zuiderveld, K.J., and Viergever, M.A. Image registration for digital subtraction angiography. *International Journal of Computer Vision*, 31:227–246, 1999. 10.1023/A:1008074100927.

[19] Moré, Jorge J. The Levenberg-Marquardt algorithm: Implementation and theory. In Watson, G. A., editor, *Numerical Analysis*, pages 105–116. Springer, Berlin, 1977.

[20] Savitzky, Abraham and Golay, M. J. E. Smoothing and differentiation of data by simplified least squares procedures. *Anal. Chem.*, 36:1627–1639, 6 1964.

[21] Schafer, Sebastian, Nol, Peter B., Walczak, Alan M., and Hoffmann, Kenneth R. Filtered region of interest cone-beam rotational angiography. *Medical Physics*, 37:694–704, 2010.

[22] Sensky, Penelope R., Samani, Nilesh J., Reek, Christine, and Cherryman, Graham R. *Cardiac Imaging*, 18:373–383, 2002.

[23] Smietanski, Marek. Convergence of a generalized newton and an inexact generalized newton algorithms for solving nonlinear equations with nondifferentiable terms. *Numerical Algorithms*, 50:401–415, 2009.

[24] Stephenson, John. Theory of the measurement of blood flow by the dilution of an indicator. *Bulletin of Mathematical Biology*, 10:117–121, 1948.

[25] Warner, Homer R. Analysis of the role of indicator technics in quantitation of valvular regurgitation. *Circ Res*, 10(3):519–529, 1962.

[26] Yoo, T., Ackerman, M., Lorensen, W., Schroeder, W., Chalana, V., Aylward, S., Metaxas, D., and Whitaker, R. Engineering and algorithm design for an image processing api: A technical report on itk - the insight toolkit. 01 2002.